3.2 | Electronic Properties

3.2.1 INTRODUCTION

The most basic chemical reaction, the transfer of a single electron, has been the subject of extensive research during the past decades. The process of electron transfer is of interest in many different scientific disciplines such as molecular biology (photosynthesis, redox enzymes…), synthetic (photo)chemistry, physics (scanning tunnelling microscopy, semiconductors), supramolecular chemistry (rotaxanes, dendrimers), or display technology (light emitting devices). More recently, major attention is being devoted to the obtaining of molecular wires that exhibit intramolecular electron transfer phenomen.[1] The interest arises from the potential use of such systems on integrated molecular devices and the technical advantages that can be derived from there.[2] First, the ever-increasing miniaturization of the architectural components of microchips reverts in the reduction size of computational systems. Second, time for an electron to travel through the circuit can be minimized using molecular-scale electronic architectures, which operate at far greater speeds. The main drawbacks are the high conformational requirements that the molecule to be used must fulfil. For instance, an average interelectrode distance of 100 Å obtained using "engineering-down" techniques; i.e. lithographic techniques, require the synthesis of molecular systems that in addition to a π-conjugated pathway, have similar dimensions to the interelectrode distance and restricted conformational geometries. Another approach, which overcomes such difficulties, is the use of self-assembling techniques. Indeed, using this technique Reed et al.[3] were able to quantitatively study the conductance of a single benzene-1,4-dithiol molecule located between two gold nanoelectrodes, as schematised in Figure 26.

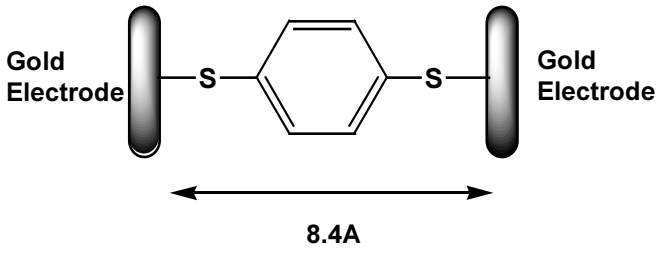

Figure 26. Single benzene-1,4-dithiol molecule located between two gold nanoelectrodes.

These results aim us to expect practical application for this kind of systems in the near future. However, before it becomes a reality, new systematic studies to obtain rules for the prediction and control of the electron propagation in molecular wires are highly required. For such studies, the use of molecular wires with donor (D) and acceptor (A) units separated by inert rigid bridges have definite advantages over freely diffusing systems.[4] The bridge not only provides a molecular skeleton to which the chromophores are add-on at well-defined separations and orientations but also provides a medium that modulates the intramolecular electron transfer (IET) dynamics by the superexchange mechanism. For these reasons, most of the experimental and theoretical studies pursued in the last two decades are based on the chemical systems and reactions given in Scheme 23.

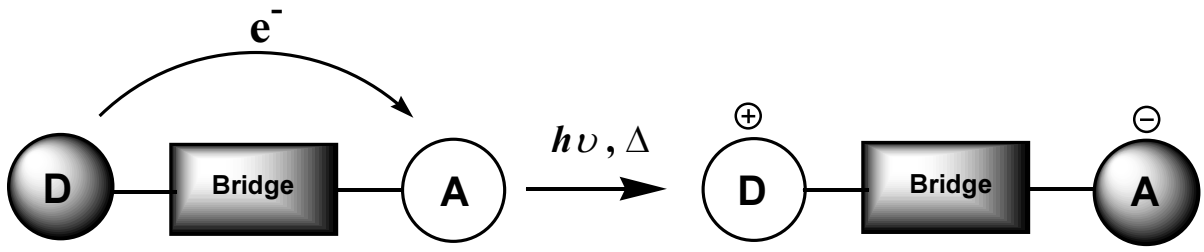

Scheme 23

Intramolecular electron transfer phenomena in Donor-bridge-Acceptor dyads may take place through three different mechanisms, which are: 1) optical self-exchange intramolecular electron transfer, 2) locally photoinduced intramolecular electron transfer and 3) thermal self-exchange intramolecular electron transfer. The three different mechanisms are schematized in Figure 27.

- *Self-exchange intramolecular electron transfer*. The essence of self-exchange electron transfer reaction is the valence interchange of two redox centers of different oxidation states (mixed-valence system). The interchange of charge requires the reorganization of the inner-shell and outer-shell environments and the energy stemming from this reorganization is related to the IET activation barrier. To overcome such barrier there are two possible mechanisms, the optical and the thermal self-exchange intramolecular electron transfer, which are schematized in Figure 27 as mechanism 1 and 3, respectively.

- *Locally photoinduced intramolecular electron transfer*. When a D-bridge-A system absorbs light whose excitation energy is localized either on the D or the A moiety (see Figure 27 mechanism 2) increasing their donor or acceptor ability (depending on the energy excitation). The locally excited state can then either decay non-productively back to the ground state or may undergo desired electron transfer to give the charge separated (CS) state. Finally the CS state inevitably undergoes charge recombination to yield the original non-excited D-bridge-A system.

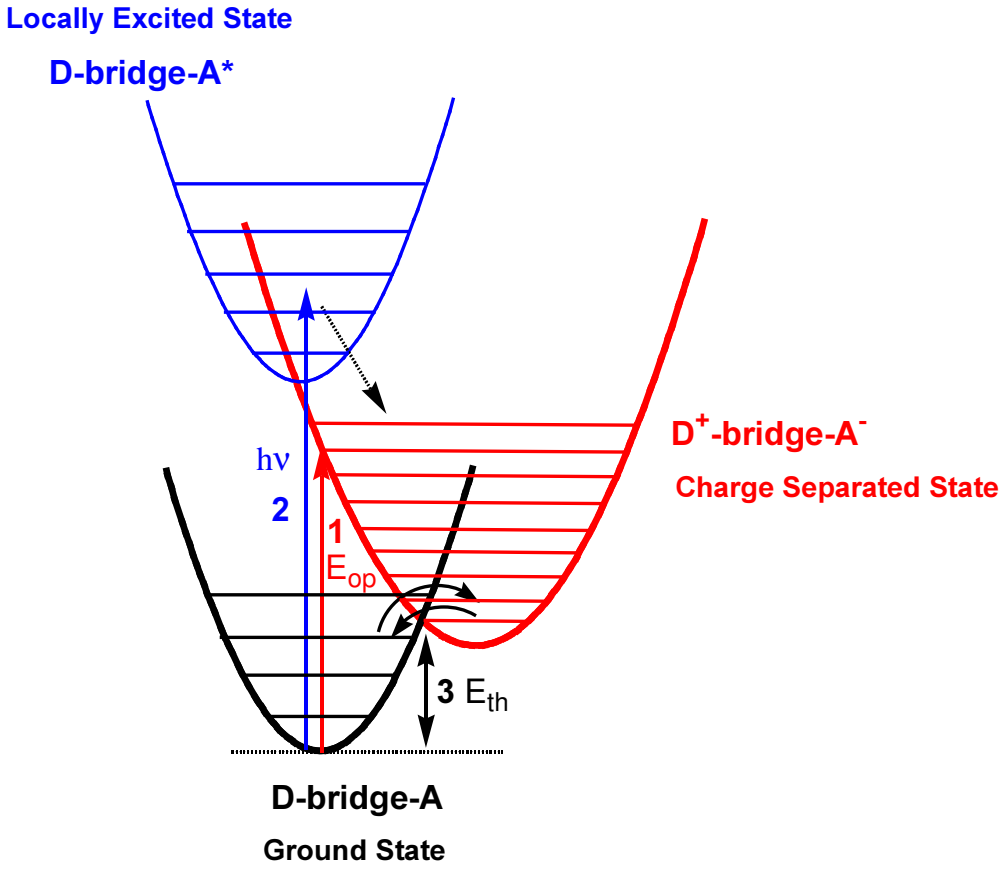

Figure 27. Schematic representation of free energy surfaces and a product and the definitions of the three mechanism fo rthe IET in D-A dyads.

3.2.1.1 Self-exchange Intramolecular Electron Transfer

Mixed-valence systems are characterized by at least two redox sites with different oxidation states linked by a bridge that mediates the transfer of electrons from one site to the other. Depending on the strength of the interaction between the redox centers, Robin and Day[5] classified the mixed-valence systems into three main different groups. In Class I the interaction between the redox centers is null. Class III systems have an electronic interaction so intense that the electron is completely delocalised all over the molecule. On the other hand in class two when the interaction between the redox centers is moderate, the electron is vibrationally localized in one of the redox centers due to the presence of an activation energy barrier (ΔG), although such barrier may be overcome by an external optical or thermal stimulus to promote an IET process (see Figure 28).

Hereby, the three different mechanisms are explained more into detail:

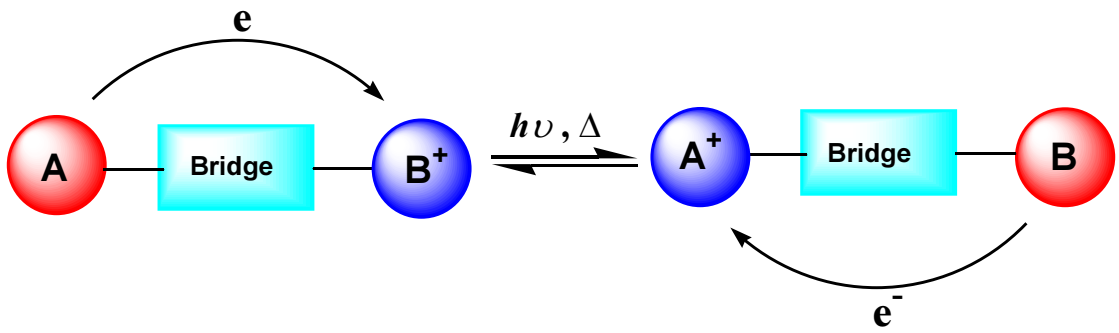

Figure 28. Schematic representation of a heteronuclear class II system where the optically and thermally induced IET process may take place.

The difference between the optical and thermal self-exchange electron-transfer processes in Class II mixed-valence systems is shown in Figure 29 (the vibrational levels have been omitted for simplicity).

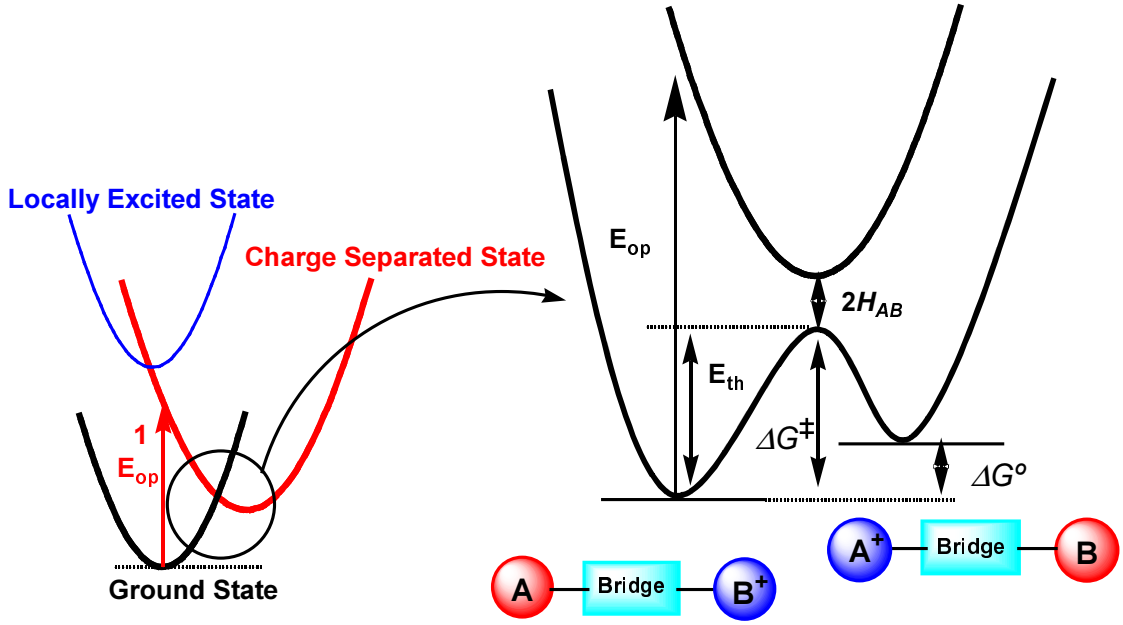

Figure 29. Potential energy curve of a heteronuclear class II system where the optically (E_{op}) and thermally (E_{th}) induced IET processes are compared and definitions of the energy difference (ΔG), the energy barrier ($\Delta G^{\ddagger}$) and the coupling parameter H_{AB}

The minimum on the left side of the curve corresponds to the equilibrium geometry of the electron when it is localized on the left side centre (A-B^+), whereas the minimum on the right side corresponds to the equilibrium geometry of the electron localized on the other centre (A^+-B). To have a thermally induced IET, the electron must move from left to right along the nuclear coordinate, without changing the electronic state, overcoming an energy barrier, E_{th}, which arises from the nuclear reorganization required before IET takes place. In other words, IET occurs through an intermediate state where bond lengths around A and B are equivalent and in between the values of both equilibrium states. When sufficient thermal

energy is available, the reaction is adiabatic and the system crosses from one energy well to another with a probability of unity. As the interaction becomes small the reaction becomes significantly nonadiabatic.

On the contrary and according with the Frank-Condon principle, optically induced IET takes place through an excited state $[A^+\text{-}B]^*$ where neither the solvent nor the internal geometry are allowed to relax. In other words, the new oxidized center, A^+, retains the bond distances and the solvation sphere of the neutral center, A, whereas the new B center retains the bond distances and the solvation sphere of the oxidized center, B^+. As a consequence intervalence band (IVB) transitions corresponding to the vertical excitation are observed in the optical absorption spectra. From the position, intensity and width of the IVB transition, which occurs generally in the near infrared region,[6] the IET can be easily characterized. In fact, the barrier E_{th} can be estimated considering two basic parameters: the vertical reorganization energy λ, and the electronic interaction matrix element H_{AB}.[7] The reorganizational energy λ is the vertical gap between the minimum on the energy surface of the precursor and the energy surface of the excited state. Such energy, λ, can be expressed as the sum of two independent contributions corresponding to the reorganization contributions of the inner (λ_i) and outer (λ_o) nuclear modes.[8,9]

$$\lambda = \lambda_i + \lambda_o \qquad \textbf{Equation 2}$$

The outer reorganizational energy, λ_o, use to be the predominant term for electron transfer processes in polar solvents and is originated by the reorientation of the solvent molecule layer around both redox centers, which differs before and after the IET takes place.[10] λ_o can be estimated from Equation 3:

$$\lambda_0 = e^2\left(\frac{1}{2a_1}+\frac{1}{2a_2}-\frac{1}{r}\right)\left(\frac{1}{\varepsilon_{op}}-\frac{1}{\varepsilon_S}\right) \qquad \textbf{Equation 3}$$

where e is the electronic charge, ε_{op} and ε_s are the optical and static dielectric constants of the solvent, a_1 and a_2 are the radii of the reactants and r is the interreactant center-to-center distance.

E_{op} is the energy required for optical electron-transfer, $\Delta G^{\neq}$ is the activation barrier for thermal electron-transfer, H_{AB} is the electronic coupling matrix between the potential energy surfaces of reactants and products, and $\Delta G°$ is the free energy difference between products and reactants. According to Marcus-Hush theory,[11] these parameters of the optical and thermal electron-transfer process are closely interrelated by the relevant equations

$$\Delta G^{\neq} = \frac{\left(\lambda + \Delta G^{\circ}\right)^2}{4\lambda} \qquad \textbf{Equation 4}$$

$$E_{op} = \lambda + \Delta G^{\circ} \qquad \textbf{Equation 5}$$

To determine the effective electronic coupling H_{AB} (expressed in cm^{-1}) between the redox sites, Equation 6 developed by Hush, can be used, [6]

$$H_{AB} = (2.05.10^{-2})\left[\frac{\varepsilon_{max}\Delta\nu_{1/2}}{\nu_{max}}\right]^{1/2}\frac{\nu_{max}}{r} \qquad \textbf{Equation 6}$$

where r is the effective separation of the two redox sites (in Å), ε_{max} is the maximum extinction coefficient (in $M^{-1}\cdot cm^{-1}$), ν_{max} is the transition energy, and $\Delta\nu_{1/2}$ is the full width at half height (both in cm^{-1}) of the intervalence absorption band.[12]

Most of mixed valence complexes that have been shown to exhibit intervalence transitions are homo or heteronuclear complexes where two metal atoms with different oxidation states are connected through an organic bridging ligand. For instance, homo and hetero nuclear metallic complexes with phenylene and/or vinylene units promoting through-bond photoinduced energy or electron transfer over considerable distances (i.e. 20Å) had already been described.[13,14] However, the flexibility of organic synthesis may allow the obtaining of pure organic molecular wires with specific and sophisticated topologies required in the highly demanding and ever-increasing world of Nanotechnology. Moreover, the study of their properties should lead to the synthesis of systems where the electron transfer could be fine-tuned in a far more precise way than had been done with coordination compounds. However, up to now, only a few examples of pure organic mixed-valence compounds showing intramolecular electron transfer phenomena have been described. Our group paid a special attention to the study of intramolecular electron transfer phenomena in pure organic mixed-valence compounds derived from polychlorotriphenylmethyl radicals. For instance, IET phenomena in the mixed-valence species derived by partial reduction of the biradical and triradical species shown in Figure 30 have been described.

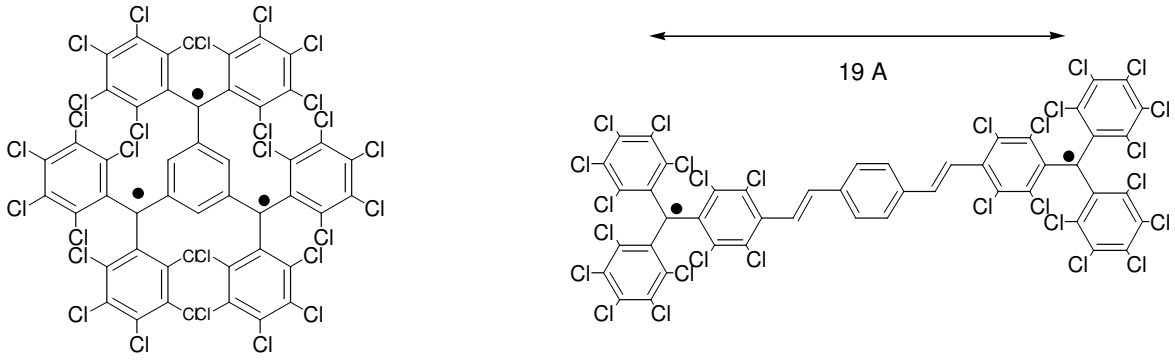

Figure 30. Triradical **a** and diradical **b** previously synthesized and studied in our group.

3.2.1.2 Locally Photoinduced Charge Separation

Absorption of light by a D-bridge-A system leads to the formation of the first excited state whose excitation energy is localized on either the D or the A moiety (see Scheme 24). [15] The locally excited state can then either decay non-productively back to the ground state or may undergo desired electron transfer to give the CS state. Finally the CS state undergoes charge recombination to yield the original nonexcited D-bridge-A system. Photoinduced electron transfer reactions are often performed in polar solvents, such as benzonitrile, in which the initial radical-ion is favoured.[16] The contact radical-ion pairs are short-lived, and if physical separation does not take place, secondary chemical reactions would have to be very rapid in order to compete with back electron transfer and other rapid first-order deactivation pathways.

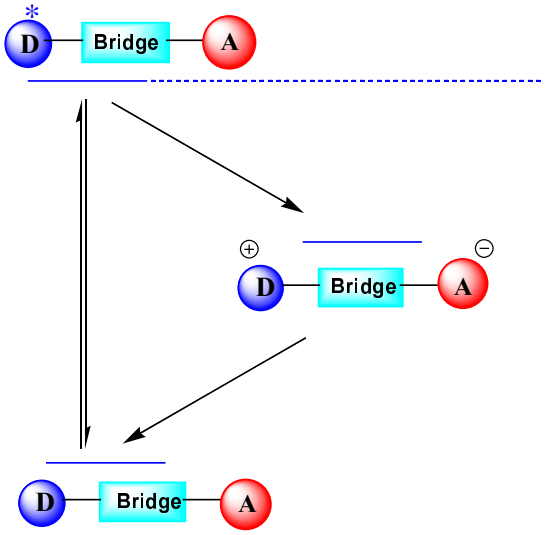

Scheme 24

To obtain the maximum efficiency for a given organic D-bridge-Acceptor system, many different approaches have been followed. One of such approaches consists in the use of a C_{60}-based chromophoric system.[17,18]

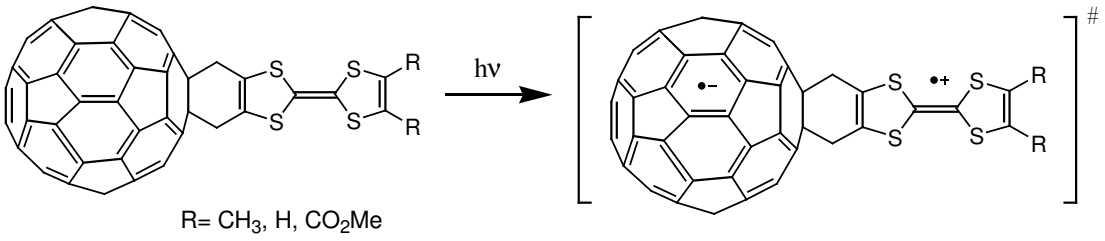

Scheme 25

Indeed C_{60} is a remarkable acceptor that accelerates photoinduced charge separation and shows a slow charge recombination in the dark. For this reason, it has been the molecule of choice to attach several electron-donor fragments to study photoinduced electron transfer., like tetrathiafulvalene (TTF) derivatives. Such chromophores are strong donor units that can be used in systems of the type D-bridge-A showing intramolecular electron transfer (Scheme 25).[19]

Another interesting system is the bichromophoric molecule shown in Scheme 26, made up of dyads with 1,4-dimethoxynaphthalene (DMN) as a donor group and rigid norbornylogous bridges or dicyanovinylene (DCV) acceptor groups. These systems provide valuable insight into the nature of long-range intramolecular charge separation and recombination processes to explore the effects of distance, bridge configuration, through-bond coupling, and orbital symmetry on long-range IET processes[20,21]

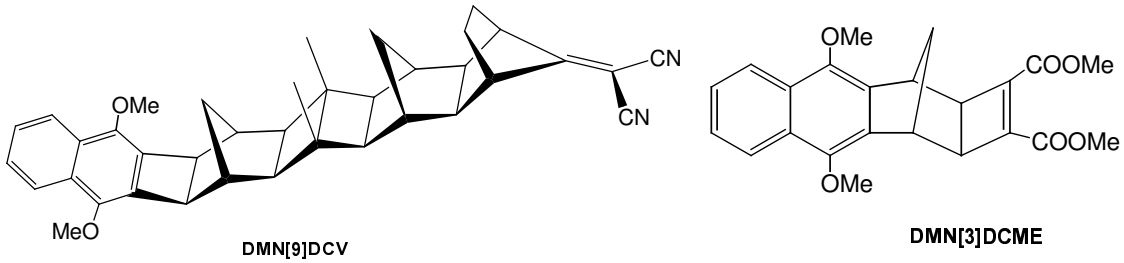

Scheme 26

One of the interesting consequences of Equation 4 is that the electron transfer rate will show different "regimes",[22] depending on the relative size of the reorganization energy and the driving force of the reaction. In Equation 4 $\Delta G^{\pm}$ will be zero when $-\Delta G^{o} = \lambda$ (optimal region) and will be larger than zero both when $\lambda > -\Delta G^{o}$ (the normal region) and when $\lambda < -\Delta G^{o}$ (the inverted region), as depicted in Figure 31. The situation shown IN Figure 31 (b) is the most common in most organic donor-πbridge-acceptor systems. In this case, the CS state is the excited state at all geometries and the lower the energy of the CS state is, the faster the decay (recombination-green arrow, energy gap) will be. This means that the recombination (green arrow) of charges in this case, takes place in the inverted region. The situation of the Figure 31 (a) is an unusual one. The CS state correlates to the ground state at a strongly distorted geometry. In this case, the recombination (green arrow) take place in the normal region and this means that the lower the energy of the CS state is, the slower the decay (activation energy) will be.

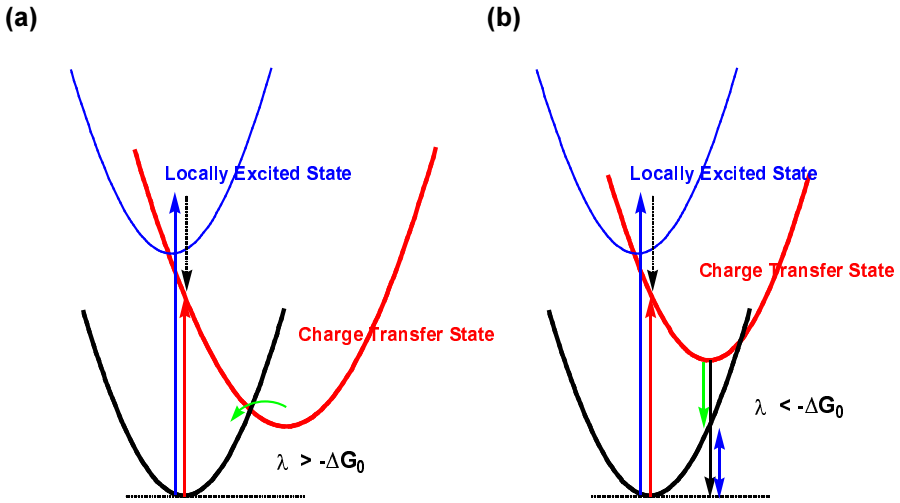

Figure 31. Schematic representation of free energy surfaces relevant in the normal region (a) and the inverted region (b)

3.2.2 RESULTS

In this chapter we will study intramolecular electron transfer phenomena in the series of radicals **1**-**5** consisting of a polychlorotriphenylmethyl radical acting as the acceptor unit and a ferrocene donor. Such IET processes may be promoted either by an external optical or thermal stimulus and are summarized at the bottom part of Scheme 27. Such studies have been developed according to the three mechanisms shown in Figure 27 through which intramoelcular electron transfer may take place. Finally, it has to be emphasized that the use of ferrocene as a donor group in molecular systems exhibiting IET is not new. For instance, prior to this work, a bimetallic complex comprising a ferrocene unit and a ruthenium metal ion with a high intervalence IET band have already been described. Recently other examples showing IET bands that have ferrocene as donor unit have been described, as that shown in Figure 32.[23]

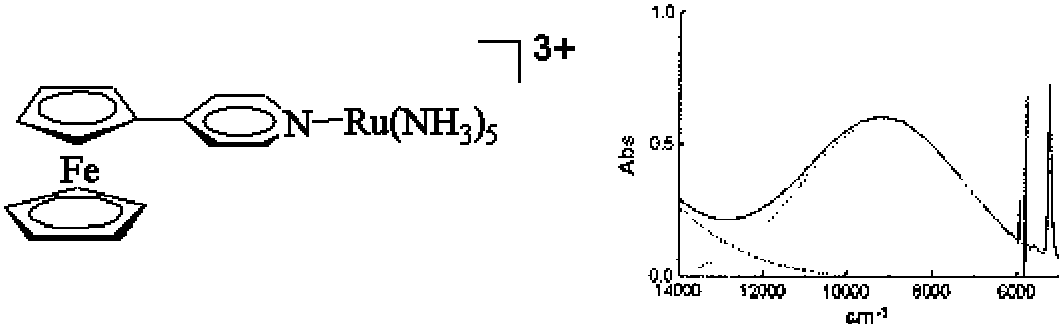

Figure 32. Intervalence band transition in the Near-IR spectra for a ferrocene-ruthenium bimetallic complex.

The main difference between the series of radicals **1**-**5** and the bimetallic complex previously described lies on the substitution of the ruthenium metal ion by an organic open-shell polychlorotriphenylmehtyl unit. This fact is expected to promote new and intriguing properties.

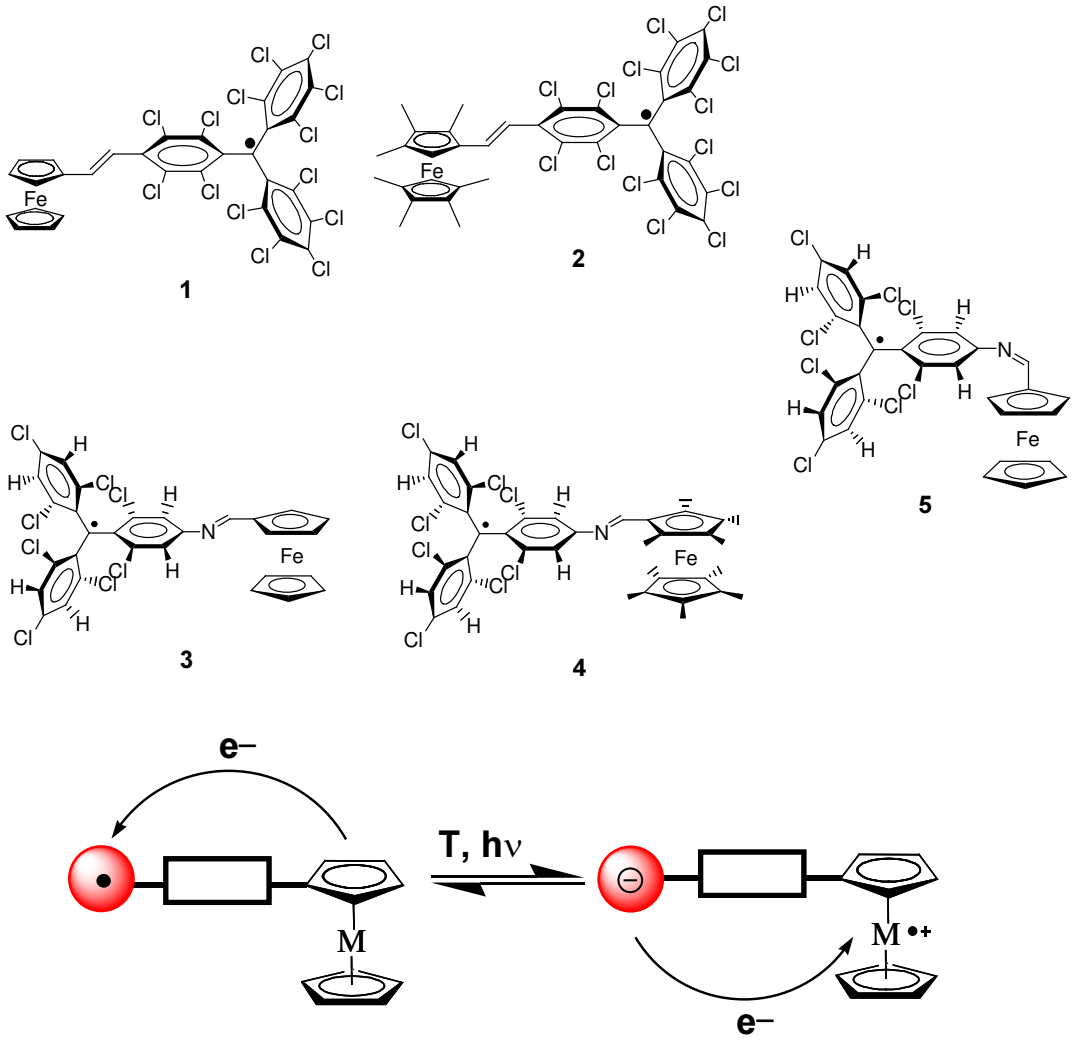

Scheme 27

General electronic considerations. Visible spectra of polychlorotriphenylmethyl radicals usually show an intense absorption band at 360 nm and two weaker bands centered between 565 and 605 nm, all of which are assigned to the radical character of the triphenylmethyl units. However, the electronic spectra of ferrocene-based polychlorotriphenylmethyl radicals exhibit a batochromic shift of the most intense band, when compared to unsubstituted chlorinated triarylmethyl radicals, due to the presence of a certain degree of electronic delocalization. Similar shifts and enhanced absorptivities have already been observed in a related *p*-divinylbenzene diradical, fact that confirms the presence of a large electronic delocalization. More interesting resulted the observation of a weak absorption in

the near-infrared region for radicals **1, 2** and **4**, which are not observed for simple polychlorotriphenylmethyl radicals neither for simple ferrocene units, whose electronic spectrum is dominated by two weak bands at 325 and 440 nm. The shorter wavelength band (λ=325 nm) is assigned to Fe(dπ) $\rightarrow$ Cp(π^*) charge transfer, $\pi \rightarrow \pi^*$ transitions, or a combination of these, whereas the longer wavelength (λ=440 nm) is assigned to a d-d transition within the ligand field formalism. It is true that upon substitution of the Cp ring with conjugated acceptors, qualitatively one would expect changes of the visible spectra. Its position and intensity depends upon the nature of the chromophore acceptor group, although shifts up to 520 nm and intensities of ε = 10000 have been reported. However, neither the position nor the intensity of the near-IR band observed for compounds **1, 2** and **4** may be assigned to intrinsic ferrocene transitions. Most likely, such band may be assigned as an intervalence band transition associated with an intramolecular electron transfer from the ferrocene unit (donor) to the radical unit (acceptor). Similar intervalence transfer bands have already been observed in mixed-valence complexes containing ferrocenyl pyridine and ruthenium ammines. Moreover, the concentration-dependence of the intervalence band follows the Beer-Lambert law, confirming the intramolecular nature of this band. As will be shown later on, the position and intensity of such band can be modulated by tuning the characteristics of the donor, acceptor and/or bridge.

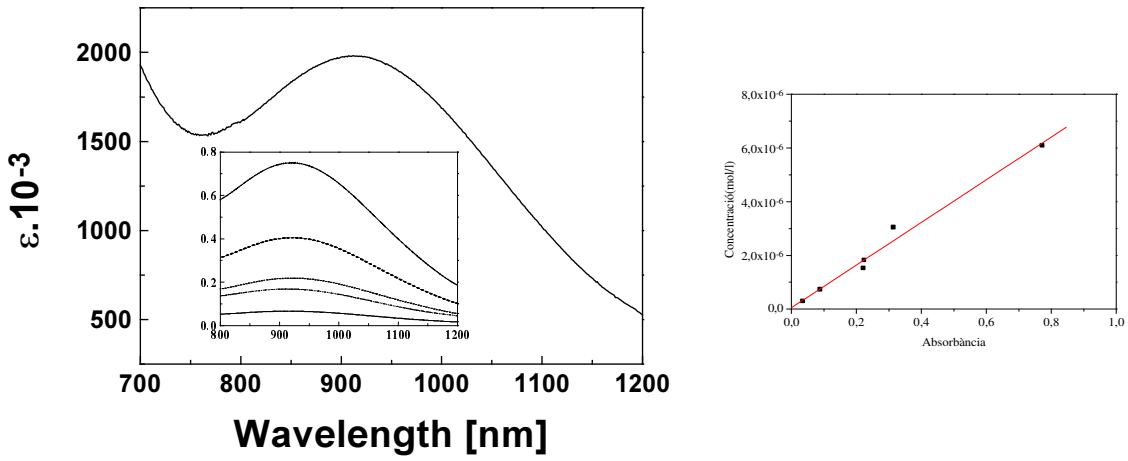

Figure 33. IET band for radical **1** in methylene chloride at different concentrations. Linear dependence of the absorbance of this band with the concentration.

Electrochemistry also offers the possibility to examine the trends in the energies of the IET processes. We have studied a range of metallocene-(π-bridge)-acceptor compounds using cyclic voltammetry in methylene chloride and 0,1M nBu$_4$N$^+$(PF$_6$)$^-$ as electrolyte and Ag/AgCl as reference electrode. The cyclic voltammetry of radicals **1-5** display two reversible redox couples, a reversible oxidation process corresponding to the Fe(II)/Fe(III) couple of the ferrocene unit and a reversible reduction process associated to the R$^\bullet$/R$^-$ couple of the radical unit and the most relevant data are given in Table 4. In compounds **1-5**, the potentials for the R$^\bullet$/R$^-$ couples occur in the range of –177mV to –670mV. These data suggest that their SOMO's are not just localized on the polychlorotriphenylmethyl group, but

also they have some contribution of the π-bridge and some influence of the metallocene unit. It is observed that by increasing the donor strength of the metallocene, by methylation of the cyclopentadienyl units; i.e., from compound **1** to **2,** it is more difficult to reduce the radical unit and the ferrocene unit it is easier to be oxidized (See Table 5). For compounds with very strong donor and acceptor units, the trends in redox behaviour are more complex due to more effective coupling between donor and acceptor.

Changes in the redox potentials for the ferrocene family of compounds indicates the presence of intramolecular electronic interactions as the redox potentials are different form the isolated chromophores. In addition it is observed the ability of modulation of the redox potential as the number of chlorines of the radical unit are changed. Thus as the number of chlorines increases the radical unit it is easier to be reduced; i.e. passing form –520mV to –130mV as we move from the partially chlorinated radical **12** to the *per*-chlorinated radical **30**. The same trend is observed when we move from compounds **3, 4, 5** to **1, 2**.

Table 5. Electochemical data for compounds **1-5, 12** and **30** in mV vs Ag/AgCl with Pt working electrode in CH_2Cl_2 and containing 0.1M Bu_4NPF_6 at 20ºC, $\Delta E_{1/2} = [(E_{½})_2 - (E_{½})_1]$

Compound	$(E_{½})_1$ (mV)	$(E_{½})_2$ (mV)	$\Delta E_{½}$ (mV)
1	-177	+587	764
2	-400	+90	490
3	-660	+610	1270
4	-600	+230	830
5	-670	+720	1390
12	-520	---	---
30	-130	---	---
Ferrocene	---	+500	---
Methylated Ferrocene	---	+200	---

In conclusion, we have seen that in all presented compounds the variation of the redox potential correlates well with the major or minor donor or acceptor ability of such compounds building blocks.

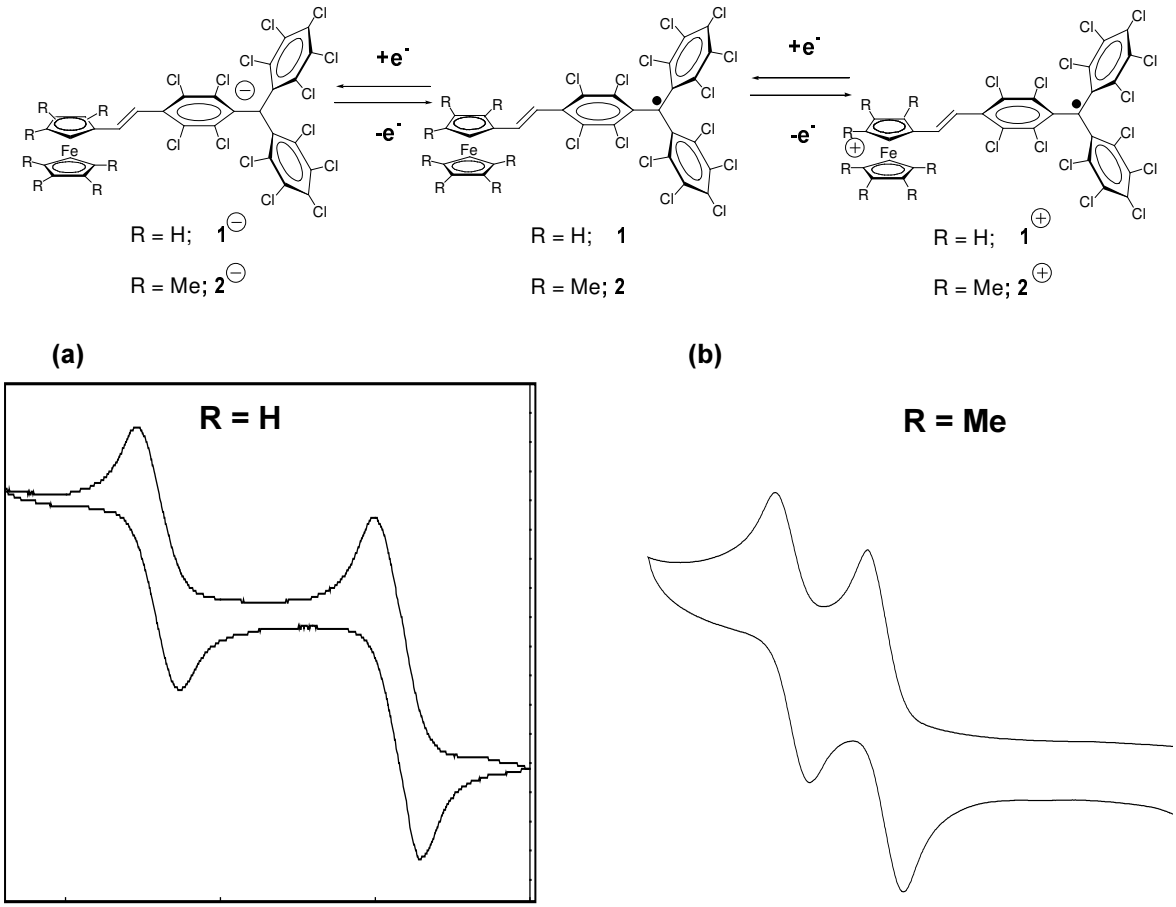

Figure 34. Cyclic voltammogram obtained from a CH_2Cl_2 solution containing NBu_4PF_6 (0.1M) of radicals (a) **1** and (b) **2**

3.2.2.1 Optically Induced Self-Exchange Intramolecular Electron Transfer

As previously described, the electronic spectra of ferrocene-based polychlorotriphenylmethyl radicals **1**-**5** in solution exhibit an intervalence band transition associated to an intramolecular electron transfer from the ferrocene group (donor) to the radical unit (acceptor). However, depending on: a) the acceptor ability of the radical unit (i.e., on the number of chlorine atoms that may confer a higher electron withdrawing character), b) the choice of the bridge, which is crucial for the good promotion of the electron delocalisation through the whole molecule, and c) the donor ability of the ferrocene (i.e.; permethylated or non-methylated), the intervalence band transiton experiences a shift towards higher or lower energies. The three different factors previously described contributing to the shift of the intervalence band are schematised in Figure 35.

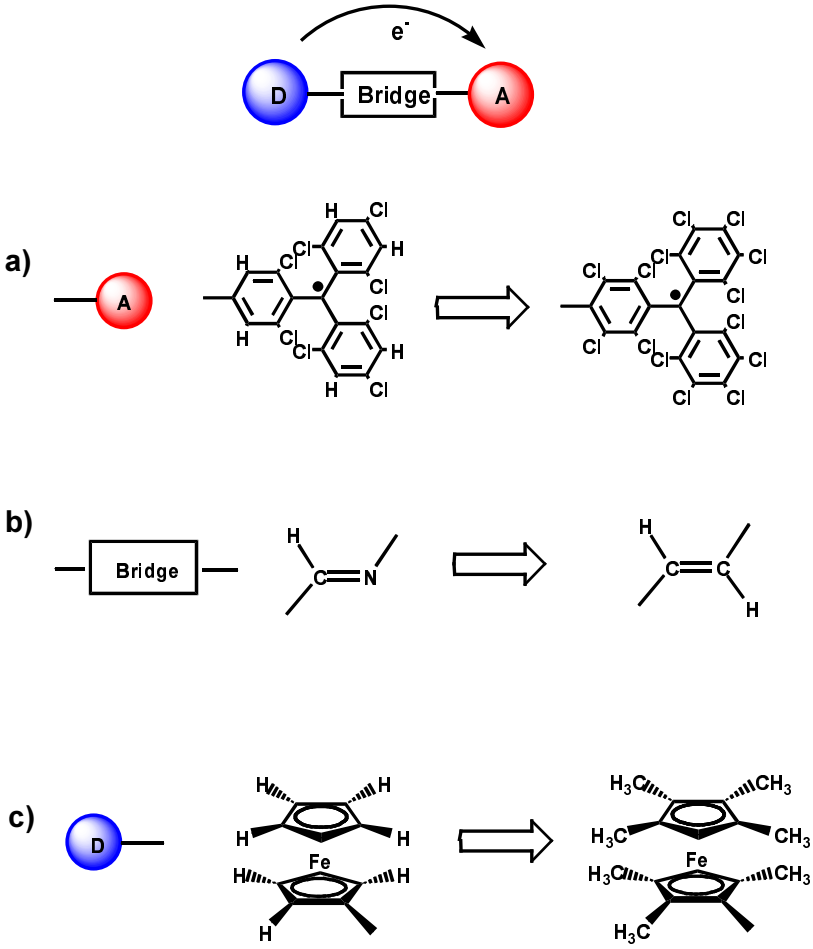

Figure 35. The three different factor governing the degree of intramolecular electron transfer between the donor and the acceptor unit in radical dyads.

Such a variation of the intervalence band is best illustrated in Figure 36. As expected, the electronic spectra of radical **2**, with a permethylated ferrocene unit and a perchlorinated triphenylmethyl unit (the strongest donor and acceptor units used in the present work), exhibits an intervalence band at the lowest energy (1477 nm). According to this situation, when the permethylated ferrocene unit is replaced by a non-permethylated ferrocene, the intervalence band experiences a hypsochromic shift to higher energies (936 nm). A related hypsochromic shift is observed for radical **4** when compared to radial **2**, where the unique variation comes from the replacement of the vinylene by an imino bridge. Finally, the electronic spectrum of radical **3** evidenced the lack of any intervalence band transition originated by an IET phenomenon. One possible reason is that the intervalence transition appears as a very broad tail on the edge of a nearby electronic transition or even completely masked since such a band is shifted to the region of higher energies.

To determinate the coupling parameters H_{AB} (effective electronic coupling between the redox sites) for coumponds **1** and **2** the Equation 6 derived from the Hush model is used.

The H_{AB} found for compound **1** and **2** are 1009 and 495 cm^{-1}, respectively. Comparing the electronic coupling found to that obtained for other species (200-300cm^{-1}) it is possible to observed that it has increased drastically.[24]

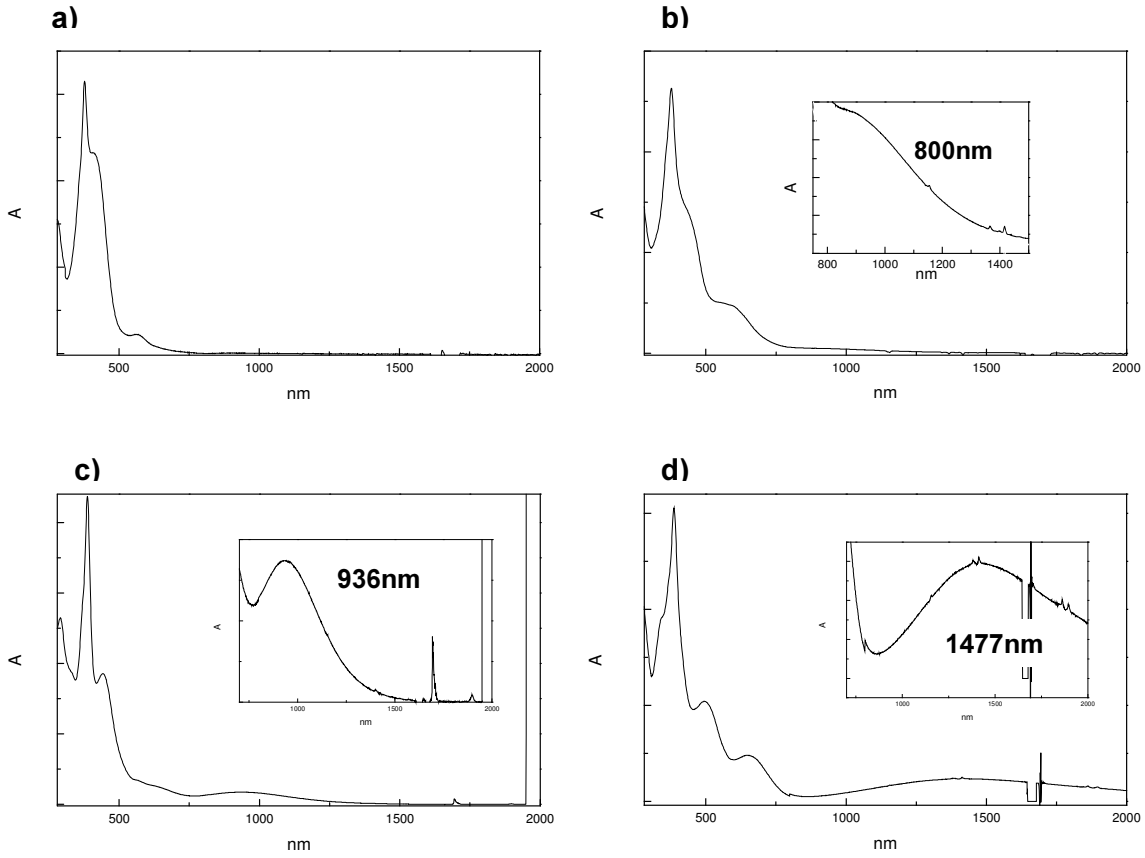

Figure 36. UV-Vis-Near IR spectra for a) **3** b) **4** c) **1** and d) **2** in methylene chloride

Linear Solvation Energy Relationshpi: A systematic study

The electronic spectra of radicals **1** and **2** were recorded in different solvents. The frequency (energy) associated to the intervalence band transition observed in the Near-IR region depends strongly on the nature of the solvent for both compounds. To better understand and identify the different solvent-solute and solvent-solvent intermolecular interactions which control this shift, we have used the Linear Solvation Energy Relationship (LSER) developed by Kamlet, Taft and co-workers. LSER is a powerful tool for the study of the principal intermolecular interactions that control a specific physicochemical process in solution, such as intramolecular electron transfer, with a free-energy change associated. LSER assumes that the different solvent/solute interactions are additive and can be categorized in two groups: the exoergic and endoergic interactions. The exoergic interactions have their origins in attractive solute/solvent interactions and can be quantified by the solvatochromic parameters π^*, α and β. These parameters can be classified in non-

specific (π*) and specific (α and β). The π* parameter measures the exoergic effects of dipole/dipole and dipole/induced dipole interactions between the solute and the solvent molecules. For some processes, when several solvents are used at the same time, a corrector term for parameter π * must be added; δ in order to have a correct polarizability for all solvents at the same time. The solvatochromic parameter α is a quantitative empirical measure of the ability of a bulk solvent to act as hydrogen-bond donor towards a solute. By contrast, the empirical parameter β measures quantitatively the ability of a bulk solvent to act as a hydrogen-bond acceptor or electron-pair donor towards a given standard solute. Finally, we have to consider the endoergic term, named cohesiveness term (Ω). This term measures the work required for separating the solvent molecules to provide a suitable sized and shaped enclosure in which the solute molecule can be accommodated. The Ω term represents the physical quantity of cohesive pressure- or cohesive energy density- of the solvent.[25]

In the present work, the specific physicochemical process in solution to be studied by the LSER approach was the shift experienced by the frequency (energy) associated to the intramolecular electron transfer band for radicals **1** and **2** when the nature of the solvent is changed. All the experiments were carried out at room temperature using 22 solvents selected to be representatives of the eleven groups in which the most common laboratory solvents have been classified.[26] As an example, the shift experienced by the intervalence band of radical **2** in different representative solvents is shown in Figure 37.

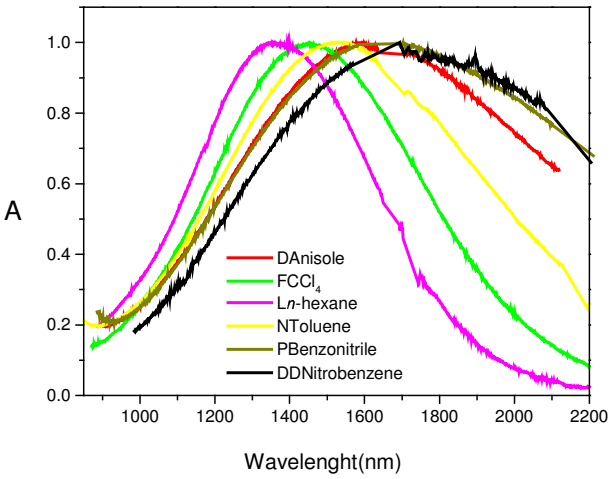

Figure 37. Near-IR Intramolecular Electron Transfer band in various solvents for compound **2**

Therefore, the generalized LSER equation that describes the intramolecular electron transfer phenomena for a ferrocene-based polychlorotriphenylmethyl radicals **1** and **2**, adopts the form of Equation 7:

$$\nu_i = \nu^\circ_i + s_i[\pi^* + d_i(\delta)] + a_i\alpha + b_i\beta + m_i\Omega \qquad \textbf{Equation 7}$$

where ν_i is the frequency (energy) associated to an intramolecular electron transfer process for a given radical (i) in a given solvent. Constant ν°_i is the frequency (energy) associated to

an intramolecular electron transfer process in absence of any solvent/solute interaction. Coefficients s_i, d_i, a_i, b_i and m_i are characteristic of each radical (i) and independent of the nature of the solvent and must have negative (or positive) signs according to the endoergic (or exoergic) nature of each term.

Table 6. Wavelenght and frequency for the IET band of radicals **1** and **2** in various solvents, and solvatochromic parameters for all the solvents used.

	Radical 1		**Radical 2**		**Solvatochormic parameters**					
Solvent	λ_{max} **(nm)**	ν_{max} **/1000 (cm^{-1})**	λ_{max} **(nm)**	ν_{max} **/1000 (cm^{-1})**	α	β	π^*	Ω**(Mpa) /1000**	δ	ξ
1. *n*-hexane	894.5	11,179	1377.5	7,259	0,001	0,00	-0,08	0,2220	0,0	0,0
2. Diethylether	936.0	10,683	1430.1	6,992	0,001	0,47	0,27	0,2280	0,0	0,0
3. Toluene	965.1	10,362	1527.3	6,547	0,001	0,11	0,54	0,3312	1,0	0,0
4. Tetrahydrofurane	971.2	10,299	1520.5	6,576	0,001	0,55	0,58	0,3459	0,0	0,2
5. CH_2Cl_2	936.2	10,684	1476.8	6,771	0,300	0,00	0,82	0,3920	0,5	0,0
6. Dimethylformamide	989.1	10,111	---	---	0,001	0,69	0,88	0,6150	0,0	0,0
7. Ethanol	974.3	10,267	---	---	0,830	0,77	0,54	0,6760	0,0	0,2
8. Dioxane	939.1	10,649	1445.6	6,917	0,001	0,37	0,55	0,4202	0,0	0,2
9. Anisol	985.2	10,152	1614.8	6,192	0,001	0,22	0,73	0,3920	0,0	0,2
10. Ethyl Acetate	952.2	10,504	1524.9	6,557	0,001	0,45	0,55	0,3459	0,0	0,0
11. Nitrobenzene	1003.3	9,970	1723.6	5,801	0,001	0,89	1,01	0,4202	1,0	0,2
12. Acetonitrile	926.0	10,799	---	---	0,190	0,31	0,75	0,5904	0,0	0,2
13. Benzonitrile	989.0	10,111	1644.7	6,079	0,001	0,41	0,90	0,2958	1,0	0,2
14. Clorobenzene	980.5	10,199	1608.5	6,217	0,001	0,07	0,71	0,3763	1,0	0,0
15. Benzene	964.0	10,373	1550.0	6,451	0,001	0,10	0,59	0,3534	1,0	0,0
16. CCl_4	925.0	10,811	1457.5	6,860	0,001	0,00	0,28	0,3097	0,5	0,0
17. Ciclohexane	912.1	10,965	1416.7	7,058	0,001	0,00	0,00	0,2822	0,0	0,0
18. Acetone	952.5	10,499	1532.0	6,527	0,080	0,48	0,71	0,4080	0,0	0,0
19. Dimethylsulfoxide	1003.0	9,9701	---	---	0,001	0,76	1,00	0,6002	0,0	0,0
20. Chloroforme	926.2	10,800	1424.9	7,017	0,440	0,00	0,58	0,3610	0,5	0,0
21. *t*-Butanol	944.5	10,588	---	---	0,680	1,01	0,41	0,4708	0,0	0,2
22. 1,2-dibromoethane	961.0	10,406	1521.6	6,571	0,001	0,00	0,75	0,4536	0,5	0,0

The frequency (energy) values of the intervalence band associated to an intramolecular electron transfer process for radicals **1** and **2** in different solvents are summarized in Table 6. As can be observed, there is a great dependence of such wavelength (frequency) with the nature of the solvent, being the maximum difference of $\Delta\lambda$ = 109nm ($\Delta\nu$ = 1.21cm^{-1}) for radical **1** and $\Delta\lambda$ = 346nm ($\Delta\nu$ = 1.46cm^{-1}) for radical **2**.

For each radical, the corresponding experimental frequency values and the solvent parameters summarized in Table 6, were fitted to Equation 7 by means of a multivariable regression method. When the multiple regression was based in a physicochemical model that includes all the solvent parameter terms (i.e.: complete Equation 7) the fit was inadequate, They did not pass any of the usual statistical test even at low confidence levels. Only models that include exclusively the independent term $\nu°_i$, the polarity term ($s_i\pi^*$) and the ability of a bulk solvent to act as a hydrogen-bond acceptor term ($a_i\alpha$) fit the data well. The resulting regresion coefficients and their corresponding statistical information are shown in Table 7.[27]

Table 7. LSER models ($\nu_i = \nu°_i + s_i[\pi^* + d_i(\delta)] + a_i\alpha$) for radical **1** and **2** describing the dependence of the frequency (energy) of the transition with the nature of the solvent.

		Coefficient (t test)[b]				Statistics				
Radical	**n[a]**	$\nu°$	a_i	s_i	d_i	**R[c]**	**S[d]**	**(r^2)[e]**	**F[f]**	**p**
1	20	11.4(0.1)	0.4(0.1)	0.3(0.1)	0.3	0.928	0.146	0.862	25.006	<0.0001
2	17	6.8(0.2)	1.3(0.2)	1.4(0.2)	0.1	0.886	0.193	0.886	25.533	<0.0001

(a)Number of data points. (b) Number in parentheses is the student's test value for the coefficient (c) Coefficient of multiple correlation (d) Standard error of the estimate value (e) Adjusted coefficient of multiple determination (f) F-test value for derived equation.

Therefore, the resulting equations are:

Radical **1**: $\nu_1 = 11.4(\pm0.1) + 0.4(\pm0.1)\,\alpha - 0.3\,(\pm 0.1)[\pi^* - 0.3(\pm0.1)\,\delta]$ **Equation 8**

Radical **2**: $\nu_2 = 6.8(\pm0.2) + 1.3(\pm0.2)\,\alpha - 1.3\,(\pm0.2)[\pi^* - 0.1(\pm0.09)\,\delta]$ **Equation 9**

The statistical results described in Table 7, indicates that the LSER models describing the dependence of the frequency (energy) of the intramolecular electron transfer transition with the nature of the solvent are valid at a significance level of α = 99.99% for both radicals. The goodness of these models, is illustrated in Figure 38 where it is shown the high concordance between the calculated and the experimental frequencies for compound **2**.

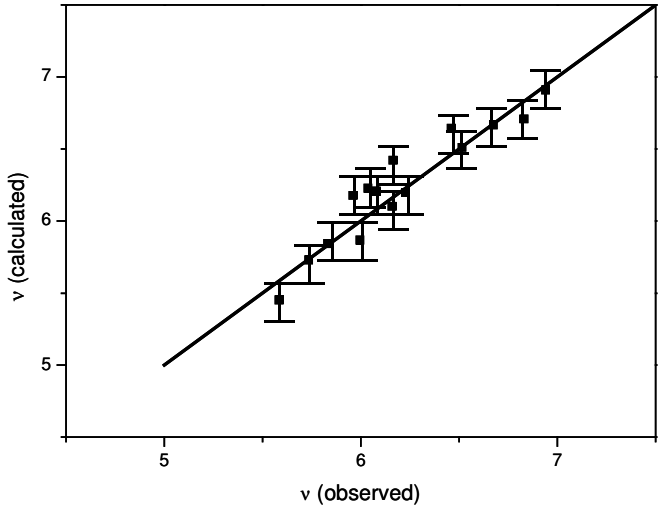

Figure 38. Calculated frequencies of compound **2**, using the LSER solubility model versus experimental values.

Finally, from the LSER analysis, the following information can be extracted:

(a) Intramolecular electron transfer phenomena have similar sensitivity to polarity changes (π^*) and changes in H-bond donor ability (α) of the solvent media, as it is inferred from the similar absolute value of the s_i and a_i coefficients.

(b) The sign of coefficient s_i is negative, showing that an increase of the solvent polarity (π^*) decreases the energy of the intramolecular electron transfer for radicals **1** and **2**.

(c) The sign of coefficient a_i is positive, indicating that an increase of the solvent H-bond donor ability (α) increases the energy of the intramolecular electron transfer phenomena.

(d) There are no solvent/solvent intermolecular interactions which affect such phenomena.

In conclusion, this study show that the energy of the intramolecular electron transfer phenomena in different solvents is not just dependent of the polarity of the solvent but also on the different Hydrogen-donor ability of the solvent. The fact that compound **2** have higher coefficients than **1** is an indication that it is much more sensitive in front of all the parameters which is probably due to the larger polarizability of **2.**.

3.2.2.2 Locally Photoinduced Intramolecular Electron Transfer

Time resolved (or transient) absorption experiments provide a very powerful tool to study the intermediate states in a photo-induced reaction. For this reason, the photophysical properties of radicals **1** and **2** were studied with such technique in deoxygenated solvents at 20ºC with a time-resolved absorption spectroscopy. (see Appendix 7.1 for more information about this technique). Neither **1** nor **2** leads to transients detectable on the nanosecond timescale, fact that might be related to the occurrence of very fast decay of the CS state by a charge recombination to the ground state. In order to investigate this in more detail we have performed picosecond transient absorption measurements in collaboration with the department of Photochemistry of the University of Amsterdam and under the supervision of Prof. A. M. Brouwer. At present the shortest excitation ("pump") wavelength available from the experimental set-up is about 350nm, which is excellently suited for the excitation of the radical chromophore to their first excitated doublet state. Employing white light probing and spectrally resolved (CCD Camera) detection the type of spectra shown in Figure 39 were obtained for both **1** and **2**.

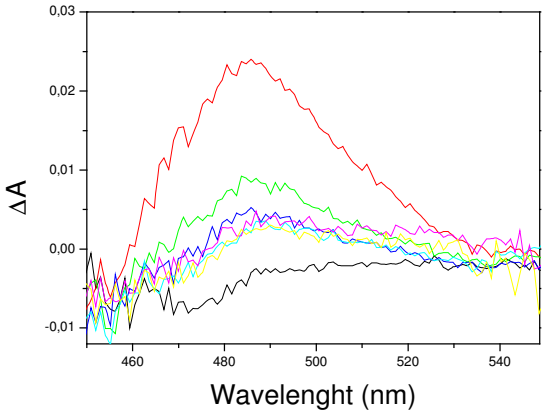

Figure 39. Transient absorption spectra of the charge separation states for **1** in CH_2Cl_2. The first spectra was 2 ps after exciting laser pulse. The time increment between the successive spectra were 0.5 ps.

These spectra, which appear immediately after excitation display the typical absorption band around 500nm that corresponds to the carbanion originated by an IET from the ferrocene unit. Then, the absorption of the cation of the ferrocene was also expected to appear around 800 nm but due to its low extinction coefficient it was not detected.

The kinetics of the CS state of radicals **1** and **2** in various solvents were investigated in more detail by single wavelength detection at 500 nm. Representative traces for compound **1** are shown in Figure 40.

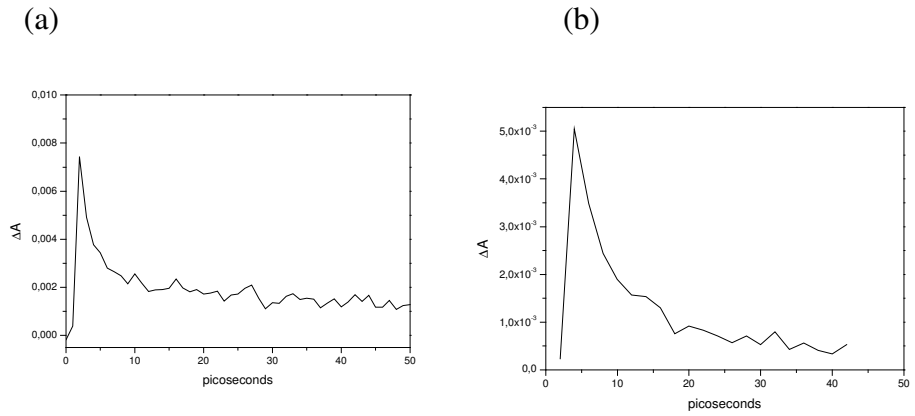

Figure 40. Transient absorption of **1** (a) benzonitrile τ = 2.9 ps (b) hexane τ = 5.5 ps. Laser excitation at 350 nm, absorption change monitored at 500nm.

The traces confirm that a CS state is formed very rapidly since the absorption rises in a period close the femptosecond time resolution available. Also the decay by charge recombination (assumed to populate the ground state directly because no intermediates are detected) occurs rapidly at a rate that indeed escapes detection on a nanosecond timescale but is readily measurable here. The decay traces can be well fitted by a single exponential curve and resulting lifetimes are compiled in Table 8.

Table 8. Dielectric constant and polarity parameters for the solvents used and life times (in picoseconds) of the charge separated states of compound **1** and **2** in various solvents

Solvent	ε	μ	Compound **1** (ps)	Compound **2** (ps)
Benzonitrile	25.20	13.51	2.9 ± 0.49	0.67 ± 0.29
CH_2Cl_2	8.93	5.17	3.4 ± 0.46	3.45 ± 0.67
EtOAc	6.02	6.27	3.3 ± 0.54	4.08 ± 0.78
Ether	4.20	4.34	4.5 ± 0.66	4.22 ± 1.06
Toluene	2.38	1.43	5 ± 0.5	3.66 ± 0.76
Hexane	1.88	0	5.5 ± 0.75	4.95 ± 0.80

3.2.2.3 Thermally Induced Self-Exchange Intramolecular Electron Transfer

In a Class II mixed-valence system the electron is vibrationally localized in one of the redox centres due to the presence of an activation energy barrier ($\Delta G^{\neq}$), although such barrier may be overcome by an external optical or thermal stimulus to promote an IET process. Here now we describe how such barrier for radical **1** may be overcome by means of a thermal stimulus (Paper IX).

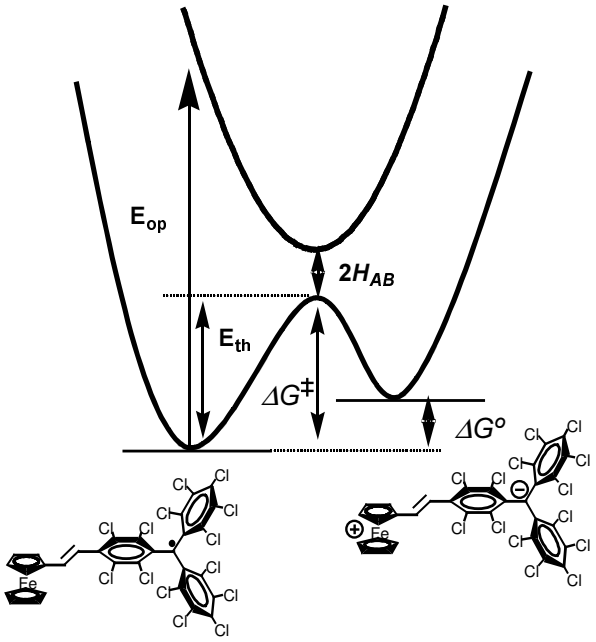

Scheme 28

To observe thermally induced IET phenomena, EPR spectroscopy is an excellent technique whenever the electron transfer rates are comparable to the experimental timescale of the EPR technique. For instance, this technique has been successfully used in our group to follow IET phenomena in the mixed-valence species derived by partial reduction of different polychlorotriphenylmehtyl biradical species. However, in the case of radical **1**, due the presence of a ferrocene unit promotes a faster relaxation, making it an EPR silent species. Nevertheless, the thermally induced IET was followed by Mössbauer spectroscopy in solid state. As shown in Figure 41, the KBr pellet of radical **1** also exhibits an intervalence band in the Near-IR region, pointing out that the intramolecular electron transfer in radical takes place not only in solution but also in solid state.

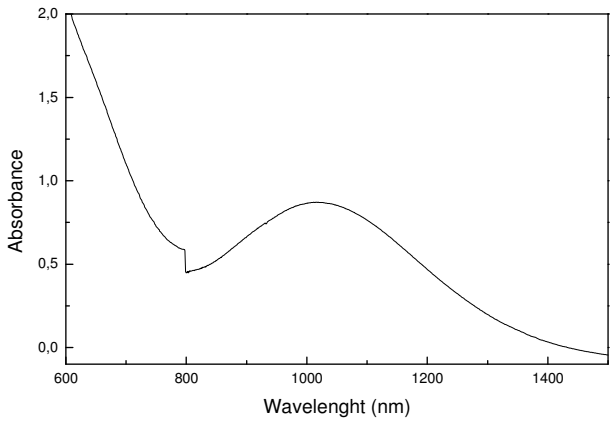

Figure 41. Near-IR Spectra of the solid at 300K

Mössbauer spectra of compound **1** have been performed with collaboration of the Department of Inorganic Chemistry of the Johannes Gutenberg-University of Mainz and under the supervision of Prof. P. Gütlich. Thus, ^{57}Fe Mössbauer spectrum of **1** in solid state exhibits a temperature dependent behaviour in agreement with a temperature dependent intramolecular electron transfer. Selected Mössbauer spectra obtained in the temperature range of 293 K to 4.2 K are shown in Figure 42. The spectrum recorded at the lowest temperature (4.2 K) shows the typical quadrupole doublet of Fe(II) ferrocene, with an isomer shift, relative to α-iron of 0.542 ± 0.002 mm s^{-1} and the quadrupole splitting being 2.337 ± 0.002 mm s^{-1}. With increasing temperature a new quadrupole doublet with a smaller splitting of 0.514 mm s^{-1}, characteristic of the ferrocenium cation, grows in at the expense of the ferrocene doublet. Clearly, this is indicative of a temperature-induced electron transfer from the ferrocene center to the radical as shown in Scheme 28. The conversion appears to be gradual up to room temperature and fully reversible, as confirmed by repetitive temperature-variable experiments. The area fraction of the ferrocenium doublet is 0.63 at 293 K and is still rising as can be seen from a plot of the area fractions as function of temperature (Figure 43).

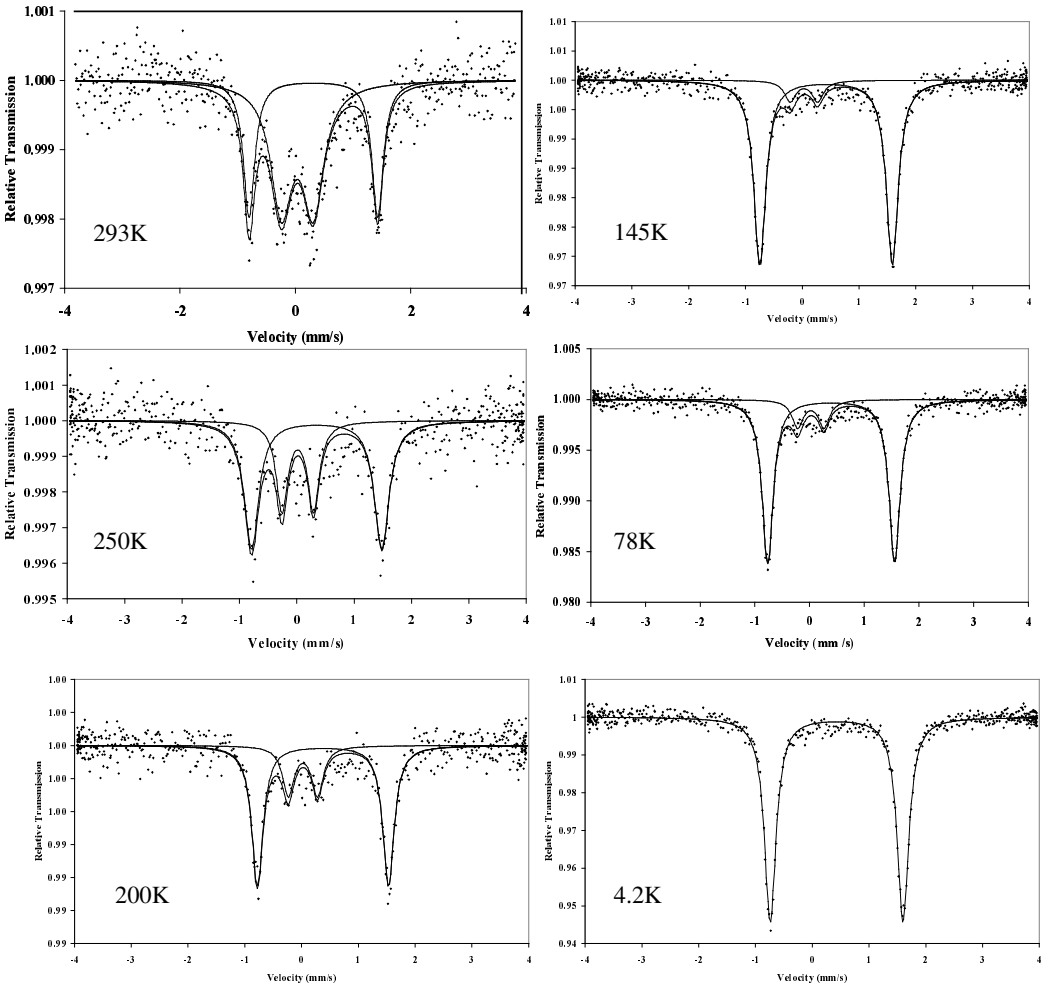

Figure 42. Fe^{57} Mössbauer spectra of radical **1** as function of the temperature.

Finally, it has to be emphasized that such a gradual interconversion was also noticed by subtle changes in the magnetization data for radical **1**. Indeed, magnetization data for radical **1** revealed that its μ_{eff} moment at 300 K was 2.28 μ_B, and recurrent measurements gave similar μ_{eff} moment values (Paper IX and Chapter 3.1).

The thermodynamic parameter, ΔH and ΔS were also determined following the methodology previously described.[28] In such a method the relative concentration of the two complexes present at each temperature is obtained by monitoring changes in spectral data intensities (see Figure 43 and Table 9).

Table 9. Relative concentration of the ferrocenium form, $\ln K_{eq}$ and ΔG in J/mol for **1** at different temperatures

T (K)	% Fe(III) species	ln K_{eq}	ΔG (J/mol)
4.2	0		
78	9	-2.313	1499.2
145	14	-1.815	2186.98
200	26	-1.0459	1738.28
250	35	-0.619	1286.05
293	64	0.575	-1400.75

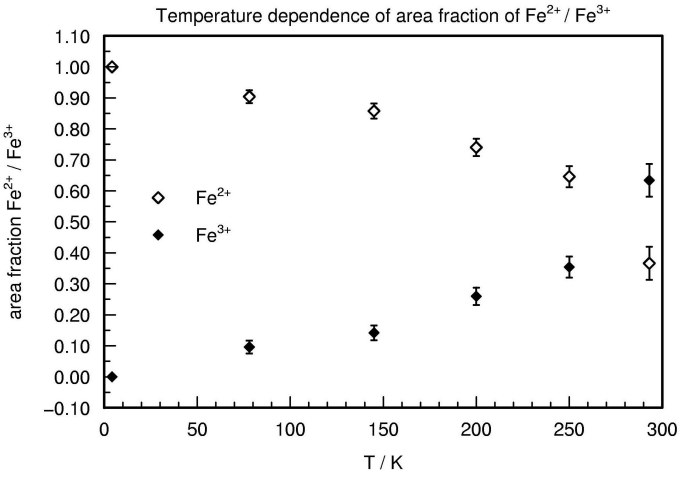

Figure 43. Plot of the Mossbauer spectra area fraction for the two species as function of the temperature.

The resulting thermodynamic parameters found are ΔH = +3294.1 J.mol^{-1} and ΔS = +11.55 J.mol^{-1}.K^{-1}. Considering that the thermal population of tautomeric isomers is dictated by the Gibbs free energy difference (ΔG) shown in Equation 10, at low temperatures, the term TΔS is negligible compared to ΔH, and consequently only the Fe(II) species are populated. However at high temperatures, TΔS is not negligible and the Fe (III) isomer becomes populated.

$$\Delta G = \Delta G_{Fe(III)\text{-}Fe(II)} = \Delta H - T\,\Delta S \qquad \textbf{Equation 10}$$

The compensation temperature *T*c of this process, at which there are equal amounts of the Fe(II) and Fe(III) forms, turns to be 285 K, which is close to room temperature.

Bistable molecular materials having two nearly degenerated states with different optical and/or magnetic properties as the one aforementioned are compounds of special interest.[29] These compounds have an appreciable sensitivity to the environment so as external perturbation, like photons or temperature, may lead to an interconversion between the two degenerated electronic states. Other examples of bistable complexes are spin-cross-over,[30,31] mixed valence,[32] and valence tautomeric bis(quinone)complexes.[3334]

Indeed, if an IET transfer process is observed for radicals **1-5**, such molecular systems may be formally considered equivalents to valence tautomeric complexes, which exhibit localized electronic structures with well-defined oxidation states for the metal and the ligands. An excellent example of this charge distribution sensitivity is exhibited by the cobalt bis(quinone) complex shown in Figure 44. Such complex interconverts reversibly between two valence tautomeric isomers: the low-spin (*ls*) and the high-spin (*hs*) with different optical and magnetic properties in response to different external perturbations such as temperature[3536], pressure or irradiation.

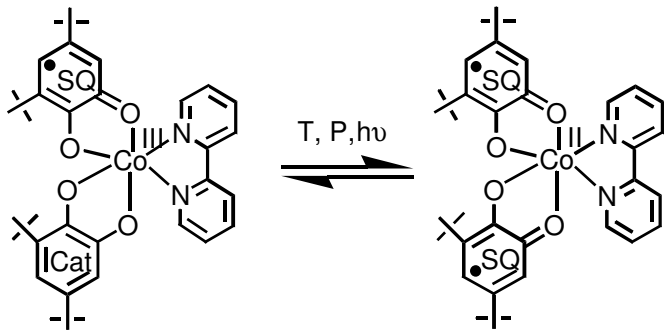

Figure 44. Valence tautomerism in a cobalt *o*-quinone complex which forms a molecular array that interconverts reversibly either by thermal, pressure or light induced means

In summary, the reversible interconversion between the two distinct electronic states of the open-shell compound **1** is thermally induced, as ascertained by Mössbauer spectroscopy. This fact entitles us to establish for the first time a new valence tautomeric compound, the radical **1**, that combines an electron acceptor organic radical unit covalently linked, through an ethylenic spacer, to a ferrocene moiety that acts as the donor group. These findings should be useful in designing novel multifunctional switchable molecular systems that can be used as information storage devices at the nanoscopic scale.

REFERENCES

1. (a) Ziessel, R.; Hissler, M.; El-Ghayoury, A.; Harriman, A. *Coord. Chem. Rev*. **1988**, *178-180*, 1251. (b) Jestin, I.; Frère, P.; Blanchard, P.; Roncali, J. *Angew. Chem. Int. Ed*. **1998**, *37*, 942.
2. (a) Tour, J. M.; Kozaki, M.; Seminario, J. M*. J. Am. Chem. Soc.* **1998**, *120*, 8486 (b) Seminario, J. M.; Tour, J. M. in Aviram Ratner (eds.) *Molecular Electronics-Science and Technology*, New York Academy of Science, New York, **1998**, p 69.
3. Reed, M. A.; Zhou, C.; Muller, C. J.; Burgin, T. P.; Tour, J. M. *Science*, **1997**, *278*, 252.
4. (a) Verhoeven, J. M.; Paddon-Row, M. N.; Hush, N. S.; Oevering, H.; Heppener, M. *Pure Appl. Chem.* **1986**, *58,* 1285 (b) Passman, P.; Verhoeven, J. W. De Boer, Th. *Chem. Phys. Lett.* **1980**, *59*, 5343 (c) Pasman, P.; Koper, N. W.; Verhoeven, J. W.; Neth, J. R. *Chem. Soc.* **1983**, *102*, 55
5. Robin, M. B.; Day, P. *Adv. Inorg. Chem. Radi. Chem.* **1967**, *10*, 247.
6. Crutchley, R. J. *Adv. Inorg. Chem.* **1994**, *41*, 273.
7. Nelsen, S. E.; Ramm, J. J.; Powell, D. R. *J. Am. Chem. Soc*. **1997**, *119*, 6863.
8. Marcus, R. A. *Angew. Chem. Int. Ed. Engl*. **1993**, *32*, 111 and refernces cited therein.
9. Sauvage, J. P.; Collin, J.-P.; Chambron, J.-C; Guillerez, S.; Courdet, *C. Chem. Rev*. **1994**, *94*, 993
10. (a) Marcus, R. A. *J. Chem. Phys*. **1956**, *24*, 966.(b) Marcus, R. A. *Annu. Rev. Phys. Chem.* **1964**, *15*, 155 (c) Marcus, R. A.; Sutin, N. *Biochim. Biophys. Acta* **1985**, *811*, 265. (d) Marcus, R. A.; Siders, P. *J. Phys. Chem.* **1982**, *86*, 622. (e) Marcus, R. A.; Sutin, N. *Inorg. Chem.* **1975**, *14*, 213. (f) Sutin, N. *J. Photochem.* **1979**, *10*, 19 (g) Hush, N. S. *Prog. Inorg. Chem.* **1967**, *8*, 391. (h) Hush, N. S. *Coord. Chem. Rev.* **1985**, *64*, 135.
11. (a) Marcus, R. A. *J. Chem. Phys.* **1956**, *24*, 966.(b) Marcus, R. A. *Annu. Rev. Phys. Chem.* **1964**, *15*, 155 (c) Marcus, R. A.; Sutin, N. *Biochim. Biophys. Acta* **1985**, *811*, 265. (d) Marcus, R. A.; Siders, P. *J. Phys. Chem.* **1982**, *86*, 622. (e) Marcus, R. A.; Sutin, N. *Inorg. Chem.* **1975**, *14*, 213. (f) Sutin, N. *J. Photochem.* **1979**, *10*, 19 (g) Hush, N. S. *Prog. Inorg. Chem.* **1967**, *8*, 391. (h) Hush, N. S. *Coord. Chem. Rev.* **1985**, *64*, 135.
12. (a) Wong, K. Y.; Schatz, P. N. *"Progress in Inorganic Chemistry"* p. 369. Wiley, New York, (b) Hush, N. S.; *"Progress in Inorganic Chemistry"* p. 391. Wiley, New York, **1983**.
13. Grosshenny, V.; Arriman, A.; Ziessel, R. *Angew. Chem. Int. Ed. Engl.* **1995**, *34*, 1100
14. (a) Patoux, C.; Launay, J.-P.; Beley, M.; Chodorowski-Kimmes, S.; Collin, J.-P.; James, S.; Sauvage, J.-P. *J. Am. Chem. Soc.* **1998**, *120*, 3717 (b) Batigelletti, F.; Flamingi, L.; Balzani, V.; Collin, J.-P.; Sauvage, J.-P-; Constable, E. C.; Cargill Thompson, A. M. W *J. Chem. Soc. Chem. Comm*. **1993**, 942. (c) Batigelletti, F.; Flamingi, L.; Balzani, V.; Collin, J.-P.; Sauvage, J.-P-; Constable, E. C.; Cargill Thompson, A. M. W. *J. Am. Chem. Soc.* **1994**, *116*, 7692.
15. Jolliffe, K. A.; Langford, S. J.; Ranasinghe, M. G.; Shephard, M. J. Paddon-Row, M. N. *J. Org. Chem.* **1999**, *64*, 1238.
16. Gould, I. R.; Farid, S. *J. Phys, Chem.* **1993**, *97*, 13067.
17. (a) Imahori, H.; Sakata, Y. *Adv. Mater*. **1997,** *9*, 537. (b) Prato, M. *J. Mater. Chem.* **1997**, *7*, 1097.
18. (a) Williams, R. M.; Koeberg, M.; Lawson, J. M.; Rubin, Y. Paddon-Row, M. N. Verhoeven, M. *J. Org. Chem.* **1996**, *61*, 5055. (b) Bell, T. D. M.; Smith, T. A.; Ghiggino, K. P.; Ranasinghe, M. G.; Shepfard, M. J. Paddon-Row, M. N. *Chem. Phys. Lett.* **1997**, *268*, 223.
19. (a) Llacay, J.; Veciana, J.. Bourdelande, J. L.; Gonzalez-Moreno, R., Vidal-Gancedo, J. Rovira, C, *J. Org. Chem*. **1998**, *63*, 5201 (b) Llacay, J.; Rovira, C.; Veciana, J. Mas, M. Molins, E. *Chem. Commun*. **1997**, 659
20. Hviid, L.; Brouwer, A. M.; Paddon-Row, M. N. Verhoeven, J. W. *Chem. Phys. Chem*. **2001**, *4*, 232.
21. (a) Clayton, A. H. A.; Ghiggino, K. P.; Lawson, J. M.; Paddon-Row, M. N. *J. Photchem. Photobiol. A-Chem.* **1994**, *80*, 323. (b) Gihggino, K. P.; Clayton, A. H. A.; Lawson, J. M.; Paddon-Row, M. N. *New, J. Chem*. **1996**, *20*, 853. (c) Paddon-Row, M. N:; Oliver, A. M.; Warman, J. M.; Smit, K. J.; Dehaas, M. P.; Oevering, H.; Verhoeven, J. W. *J. Phys. Chem*. **1988**, *92*, 6958.
22. Sutin, N; Marcus, R. A.; *Biochim. Biophys. Acta* **1985**, *811*, 265
23. Malaun, M.; Reeves, Z. R.; Paul, R. L.; Jeffery, J. C.; McCleverty, J. A.; Ward, M. D.; Asselberghs, I.; Clays, K.; Persoons, A. *Chem. Commun*. **2001**, 49.
24. (a) Chen, Y. J.; Kao, C.-H.; Lin, S. J.; Tai, C.-C.; Kwan, K. S. *Inorg. Chem*. **2000**, 39, 189 (b) Neyhart, G.; Hupp, J. T.; Curtis, J. C.; Timpson, C. J. Meyer, T. J. *J. Am. Chem. Soc*. **1996**, *118*, 3724

25. Hilderbrand, J. H.; Scott, R. L. "The solubility of Non-Electrolytes", 3ed, Dover Publications, New York, **1964**, 424
26. Ventosa, N.; Ruiz-Molina, D.; Sedó, J.; Rovira, C.; Tomas, S.; André, J-J.; Bibier, A ; Veciana, J. *Chem. Eur. J.* **1999**, *5*, 3533-3548.
27. (a) SYSTAT for windows, Version 5, SYSTAT, Inc., Evanston, Illinois, **1992**. (b)J. Neter, Wasserman, W.; Kunter, M.;" Applied linear statistical models" 2nd Ed., Richard E. Irwin, Inc., Homewood, Illinois, **1985** (c) Velleman, P. F.; Welsh, R. E *The Americal Statistician*, **1981**, 35, 234.
28. (a) Pierpont, C. G.; Jung, O. S. *Inorg. Chem*. **1995**, *34*, 1481. (b) Jung, O. S.; Pierpont, C. G. *Inorg. Chem*. **1994**, *33*, 2227.
29. Kahn, O.; Launay, J. P., *Chemtronics*, **1988**, *3*, 140.
30. (a) Hauser, A. *Comments Inorg. Chem.* **1995**, *17*, 17 (b) Hauser, A.; Vef, A.; Adler, P. *J. Chem. Phys.* **1991**, *95*, 8710.
31. (a) Gütlich, P.; Hauser, A.; Spiering, H., *Angew. Chem. Int. Ed. Engl.* **1994**, *33*, 2024 (b) Kahn, O.; Jay-Martinez, C. *Science*, **1998**, *279*, 44.
32. (a) Creutz, C. *Prog. Inorg. Chem*, **1983**, *30*, 1 (b) Richardson, D. E.; Taube, H. *Coord. Chem. Rev.* **1984**, *60*, 107.
33. Wheeler, D. E.; Rodriguez, J. H.; McCusker, J. K., *J. Phys, Chem. A* **1999**, *103*, 4101 (b) Pierpont, C. G.; Lange, C. W. *Prog. Inorg. Chem.* **1994**, *41*, 331.
34. (a) Ruiz-Molina, D.; Veciana, J.; Wurst, K.; Hendrickson, D N.; Rovira, C. *Inorg.Chem*. **2001**, *39*, 617 (b) Ruiz-Molina, D.; Wurst, K.; Hendrickson, D. N.; Rovira, C.; Veciana, J. *Adv.Funct.Mater.* **2002**, *2,* 347